Electric Double Layer Capacitance on Hierarchical Porous Carbons in an Organic Electrolyte

Hirotoshi Yamada,[a,*] Isamu Moriguchi [a], Tetsuichi Kudo [b]

[a] Faculty of Engineering, Nagasaki University,

1-14, Bunkyo-machi, Nagasaki, 852-8521, Japan

[b] National Institute of Advanced Industrial Science and Technology

Tsukuba Central 2, 1-1-1, Umezono, Tsukuba, 305-8568, Japan

* To whom correspondence should be addressed.

Dr. Hirotoshi Yamada

Faculty of Engineering, Nagasaki University

1-14, Bunkyo-machi, Nagasaki, 852-8521, Japan

Phone/Fax: +81-95-8192861

E-mail: h-yama@nagasaki-u.ac.jp

Abstract

Nanoporous carbons were prepared by using colloidal crystal as a template. Nitrogen adsorption/desorption isotherms and transmission electron microscope images revealed that the porous carbons exhibit hierarchical porous structures with meso/macropores and micropores. Electric-double-layer-capacitor performance of the porous carbons was investigated in an organic electrolyte of 1 M $LiClO_4$ in propylene carbonate and dimethoxy ethane. The hierarchical porous carbons exhibited large specific double layer capacitance of c.a. 120 F g^{-1} due to their large surface areas. In addition, the large capacitance was still obtained at a large current density up to 10 A g^{-1}, which satisfies demands from the high power application such as hybrid electric vehicles. Capacitance analysis of the hierarchical porous structures revealed the contribution of meso/macropores and micropore to the electric double layer capacitance to be 8.4 and 8.1 μF cm^{-2}, respectively. The results indicated electric double layer is formed even when solvated ions are larger than pore diameters.

Keywords: Porous carbon; Micropore; Electric double layer capacitor, Organic electrolyte; Hierarchical pore

1. Introduction

Electric double layer capacitors (EDLCs) with both large energy density and large power density have been strongly demanded especially from the viewpoint of application to auxiliary power sources of hybrid electric vehicles (HEVs) or fuel cell electric vehicles (FCEVs). Energy density of EDLCs is given by a formula: $1/2\ CV^2$ where C and V is capacitance and cell voltage, respectively. To increase the energy density, porous carbons with large surface, e.g., activated carbons, area are widely used. Double layer capacitance depends not only on surface areas of the porous carbons,[1] but also on pore sizes,[2-4] functional groups,[5] orientation of graphene layers,[6,7] and so on. Micropores (d < 2 nm, d being a pore diameter) exhibit large specific surface areas but ion transportation may be interfered by pore walls, which means poorer power density. And especially when pore diameters are smaller than solvated ions, the formation of double layer is supposed to be impossible. We have so far prepared porous carbons by a colloidal-crystal-templating method using phenolic resin as a carbon source.[8,9] This class of carbons attracts our interests not only because they possess large specific surface areas, but also because they exhibit two distinct pore size distributions: one is in the region of mesopores (2 nm ≤ d < 50 nm) or macropores (d ≥ 50 nm), which is originated from template SiO_2 particles, and the other is in the region of micropores, which is derived from carbonization of the phenolic resin. In other words, these porous carbons possess a hierarchical porous structure: micropores exist on pore walls of

meso/macropores. For such a porous structure, electrolyte ions can be delivered smoothly through meso/macropores to micropore surfaces with large specific surface areas. The hierarchical porous structure is also of importance from a fundamental viewpoint because it allows us to analyze contribution to capacitance by meso/macropores and micropores, separately. In the case of activated carbons or typical mesoporous carbons,[10,11] pore sizes are continuously distributed from micropore to mesopore regions, which make the analysis complicated. In addition, electrolyte transport in their narrow pores cause the kinetic polarization and thus capacitance may be underestimated. In the previous study, we reported that in an aqueous electrolyte (1 M H_2SO_4), contribution of micropores to the double layer capacitance was almost negligible,[9] which may not be surprising because the solvated ions are as small as pore sizes.

Another way to achieve high-energy EDLCs is to employ organic electrolytes instead of aqueous electrolytes, because they exhibit wider potential windows,[12] and accordingly increase maximum cell voltage (V) from c.a. 1 V to c.a. 2~2.5 V. However, organic electrolytes exhibit some drawbacks in contrast to aqueous electrolytes: e.g., poorer electrolyte conductivity (typically ~10 mS cm^{-1}) due to their viscous solvent [12] and smaller specific double layer capacitance (2~10 μF cm^{-2}).[13] Structure of double layer in organic electrolytes might be different from that in aqueous electrolytes. Chmiola et al. reported that micropores with diameters smaller than 1 nm exhibit larger specific capacitance than larger

pores in a non-aqueous electrolyte.[14] The results are against the commonly accepted concept that such micropores hardly contribute to capacitance, and they proposed that the structure of double layer in very small pores are different from that in relatively large pores. In this context, we investigated the double layer capacitance of the hierarchical porous carbons in an organic electrolyte.

2. Experimental

Porous carbons were synthesized by following the same procedure as reported.[8,9] First, colloidal crystal templates were fabricated by centrifugation of mono-dispersed SiO_2 colloid (particle diameter, *d*: 8, 17, 45, 110 nm, Catalysis & Chemicals Co. Ltd.). Then, a mixture of phenol, formaldehyde (37%), and a small portion of hydrochloric acid was impregnated into interstices of the SiO_2 particles. After polymerization of phenol and formaldehyde and subsequent carbonization of the phenolic resin at 1,000 ºC in Ar flow for 5 h, nanocomposites of SiO_2 and carbon was obtained. Finally, SiO_2 was removed by a hydrofluoric acid (46 wt-%) and meso/macroporous carbons were obtained. Hereafter, the porous carbons thus obtained is referred to as C[d_{SiO2}] where d_{SiO2} is the particle size of the template SiO_2 colloid. In this study, two specimens were fabricated for each d_{SiO2} in order to check the reproducibility. They are distinguished with a suffix "-1" or "-2".

The residual SiO_2 in the nanoporous carbons was confirmed by thermalgravimetry and

differential thermal analysis (TG-DTA) on a TG/DTA6300 (Seiko Instruments Inc., heating rate: 10 K min^{-1} in an air flow). To investigate carbon structure, X-ray diffraction (XRD) patterns were recorded on a RINT-2200 (Rigaku, with irradiation of Ni-filtered CuKα) and Raman spectra were measured on an RMP-210 (JASCO, with a 532-nm laser). The porous structure of carbons was observed by transmission electron microscopy (TEM, JEOL JEM-2010). Pore parameters were obtained by the analysis of nitrogen adsorption-desorption isotherms recorded at 77 K on a BELSORP-mini (BEL Japan, Inc.). Total specific surface area (S_{total}) was determined by analyzing α_{SPE}-plots based on the subtracting pore effect (SPE) method. The specific surface area of meso- and macropores (S_{meso}) was analyzed by using *t*-plots. The specific surface area of micropores (S_{micro}) was estimated by subtracting S_{meso} from S_{total}. Pore size distribution was obtained from the adsorption branches of the isotherms using the Barrett-Joyner-Halenda (BJH) method for mesopores and the Horvath-Kawazoe (HK) method for micropores.

Electrochemical properties were examined in a 1 M $LiClO_4$ solution in a mixed solvent of propylene carbonate (PC) and dimethoxy ethane (DME) (1:1 by volume) in a potential range from 2.0 to 4.0 V vs. Li/Li^+ at 25 °C by using three-electrode cells. Cyclic voltammetry and galvanostatic charge/discharge tests conducted on electrochemical analyzers S1470E (Solartron Analytical Inc.) and HJ-SM8 (Hokuto Denko Corp.), respectively. The charge/discharge tests employed the constant-current and subsequent constant-voltage

(CC-CV) mode. Electric double layer capacitance (C_{DL}) of nanoporous carbons was obtained as the differential capacitance from the slope of the galvanostatic charge/discharge tests. For the electrochemical measurements, mixtures of the porous carbons and poly(tetrafluoroethylene) (10:1 by mass) that were pressed onto Ni nets served as working electrodes. Both reference and counter electrodes employed metallic lithium pressed on Ni nets. The reference electrode was placed about 0.5-1.0 mm away from the working electrode by using Luggin-capillary. The working electrodes were immersed in the electrolyte in vacuo beforehand. The cell was assembled in an Ar-filled grove box in which H_2O concentration was kept below 1 ppm.

3. Results and Discussions

TG analysis demonstrated that residual SiO_2 in the porous carbons was less than 3 %. According to elemental analysis, atomic ratio of H to C of the porous carbons was about 0.1-0.15, and was much smaller than that of original phenolic resin (0.93), which indicates the progress of the carbonization. In Raman spectra (not shown), two peaks were observed around 1,340 and 1,580 cm^{-1} for all the porous carbons, which are the so-called D-band and G-band of carbonaceous materials, respectively. In XRD profiles, very broad peaks appeared around 25º and 44º due to the poor crystallinity, which are typical of so-called hard carbons.

Figure 1 shows that the N_2 adsorption/desorption isotherms of the porous carbons C[d_{SiO2}].

All the isotherms exhibited steep increases of N_2 uptake at relative pressures above 0.6, and the onset pressure of the increase shifted towards higher relative pressure with increasing d_{SiO2}, which indicates that the specimens possess meso/macropore and the pore diameter increases with increasing d_{SiO2}. The mesopore size distributions of the porous carbons are plotted in Fig. 2(a), which clearly demonstrated that the pore diameters corresponded to the template SiO_2 sizes. TEM images also confirmed that spherical meso/macropores with the same diameter as d_{SiO2} were successfully formed as shown in Fig. 3(a)-(c). Figure 2(b) exhibits the micropore size distributions, which exhibited a peak around 0.7 nm. This peak pore size was independent of d_{SiO2}. In a high resolution TEM image (Fig. 3(d)), the micropores smaller than 1 nm were confirmed on meso/macropore walls. These micropores possibly result from the carbonization of the phenolic resin as mentioned in the introduction. Based on these results, the hierarchical porous structure is schematically illustrated in Fig. 4. Specific surface areas of the porous carbons are summarized in table 1. One may expect that the meso/macropore surface area, S_{meso}, increase with decreasing d_{SiO2}, if the carbons were synthesized with a template of closest-packed spherical SiO_2 particles. No clear trend of S_{meso}, however, was obtained, which indicates the disordered meso/macroporous structures for small d_{SiO2}, which were observed in TEM images (Fig. 3(c,d)).

Figure 5 displays cyclic voltammograms of the hierarchical porous carbons. The differential capacitance was almost rectangular and independent of electrode potential,

whereas voltammograms in aqueous electrolyte exhibited a peak around potential of zero charge (E_{pzc}). This means that no faradaic reaction and no potential dependent ion penetration occur in an organic electrolyte.

Figure 6 displays the charge/discharge curves of the porous carbons obtained by CC-CV mode. For all the porous carbons, almost straight lines were obtained when constant currents were applied. Table 1 summarizes electric double layer capacitance, C_{DL}, obtained from slopes of charge curves (2.0 V to 4.0 V vs. Li/Li^+). Large C_{DL} of 119 F g^{-1} at 0.05 A g^{-1} was obtained for the porous carbons with S_{total} of 1455 m^2 g^{-1} (C[17]-2), which followed the relationship reported by Lozano-Castelló et al.[13] Larger C_{DL} would be expected for a porous carbons with large surface area which would be obtained by optimizing the fabrication procedure. As summarized in table 1, series resistance, R_s, which was extrapoltated from the charge curves at 5 A g^{-1} increased with decreasing d_{SiO2}. R_s is mainly attributed to the electrolyte resistance through the pores. The charge/discharge curves exhibited almost the same slopes, indicating the effective surface areas in double layer capacitance didn't decreased even at a large current density of 10 A g^{-1}. C_{DL} at 5 A g^{-1} was almost the same as that at 0.05 A g^{-1} (see table 1). To the contrary, for typical activated carbons, capacitance decreased to 20-60% of the initial capacitance when current density was increased to 2 A g^{-1}.[15] The very good rate capability of the hierarchical porous carbons is attributed to their meso/macropores which facilitate ion transport to whole surfaces. The rate capability of the

EDLC performance of the hierarchical porous carbons will be discussed in detail in a future article.

The contribution of meso/macropores and micropores to C_{DL} were analyzed by using the following equation:[1,9]

$$C_{DL} = c_{dl,meso} \cdot S_{meso} + c_{dl,micro} \cdot S_{micro} \quad (1)$$

or

$$\frac{C_{DL}}{S_{micro}} = c_{dl,meso} \cdot \frac{S_{meso}}{S_{micro}} + c_{dl,micro} \quad (2)$$

where $c_{dl,meso}$ and $c_{dl,micro}$ are specific electric double layer capacitance on meso/macropores and micropores, respectively. In Fig. 7, which plots C_{DL}/S_{micro} versus S_{meso}/S_{micro}, a linear relationship was clearly observed. By comparing the line and Eq. (2), $c_{dl,meso}$ and $c_{dl,micro}$ were estimated to be 8.4 μF cm^{-2} and 8.1 μF cm^{-2}, respectively. It should be noted that $c_{dl,micro}$ is not negligible in the organic electrolyte, and even comparable to $c_{dl,meso}$. On the other hand, in an aqueous electrolyte of 1 M H_2SO_4, $c_{dl,meso}$ was c.a. 22 and $c_{dl,micro}$ that depended on the electrode potential, E, was 5-10 μF cm^{-2} around E_{pzc} and 0-5 μF cm^{-2} off E_{pzc}.[9] The difference in the capacitance contribution between the aqueous electrolyte and the organic electrolyte might indicate the different electric double layer structures: the thickness of the Helmholtz layer and the diffusion layer, the viscosity of the solvent, and the wettability of surfaces, and so on.

Let us now discuss the size of solvated ions and pores. In the cyclic voltammograms (Fig.

5), the differential capacitance was slightly higher for potential range $E > E_{pzc}$ (~ 3.0 V vs. Li/Li^+) than $E < E_{pzc}$. For the former potential range, perchlorate ions are mainly accumulated in double layer whereas for the latter, lithium ions are attracted to electrode surfaces. One might suppose that this is caused by the ion sieving effect by micropores,[16] i.e., the Stokes' radius of lithium ions (0.41 nm in PC) is larger and that of perchlorate ions (0.26 nm) is smaller than the peak radius of the micropores (0.35 nm),[17] and thus, lithium ions cannot form double layers in micropores. In this case, the capacitance would be related to micropore ratio (S_{micro}/S_{total}). However, this model is denied by the fact that S_{micro}/S_{total} was distributed in the range from 25 to 60% for all the porous carbons, whereas the capacitance difference $C_{DL}(E < E_{pzc})$ and $C_{DL}(E > E_{pzc})$ was c.a. 25% and less dependent on the specimens. The capacitance difference would be simply explained by the thickness of the Helmholtz layer: the Helmholtz layer is thinner and specific capacitance is larger for ClO_4^- than for Li^+. This means the ions can be accumulated even in the micropores that are smaller than their sizes. These results agree with that reported by Chmiola et al: in small pores the compressed electric double layer is formed with distorted ions.[14] According to them, C_{DL} for such compressed double layer exhibit larger values than in larger pores without double layer compression, although $c_{dl,micro}$ was comparable to $c_{dl,meso}$ in this work. There may be two plausible origins of the distorted ions: distorted structure of solvated Li^+ ion, or partially desolvated Li^+ ion. Electrochemical impedance spectra (EIS, not shown) support the distorted structure of

solvated Li^+. According to Ue, Li+ in PC is supposed to form solvated ion with surrounding PC molecules due to its large charge density, whereas solvation of ClO_4^- is almost negligible.[17] In addition, it is reported that partial desolvation of lithium ions require an additional process.[18,19] However, EIS obtained above and below E_{pzc} (corresponding to accumulation of ClO_4^- and Li^+, respectively) did not exhibited obvious difference, which means that no additional process occurs when Li^+ enters micropores. On the other hand, as for aqueous solution, partial desolvation is reported.[20] However, water is different from organic solvents because water molecules tend to form a highly ordered structure in the carbon nanospaces.[21] Capacitance in compressed double layer would be further investigated in a future study by using different electrolytes with various ion sizes or by using porous carbons with different micropore sizes.

4. Conclusions

In this paper, we investigated electric double layer capacitance of the hierarchical porous carbons in an organic electrolyte. The porous carbons exhibited large specific double layer capacitance of 120 F g^{-1} in an organic electrolyte of a 1 M $LiClO_4$/(PC+DME) due to their large surface areas, and superb rate capability resulting from interconnected hierarchical porous structures. The results satisfy the demands for EDLCs for high-power applications such as HEVs. The hierarchical porous structures also revealed the contribution of

meso/macropores and micropore to the electric double layer capacitance, separately. The specific capacitance of meso/macropores and micropores were 8.4 and 8.1 μF cm^{-2}, respectively. The results indicated electric double layer is formed even when solvated ions are larger than pore diameters.

Acknowledgements

Authors thank Mr. H. Furukawa for TEM operation. We gratefully acknowledge helpful comments of Dr. I. Honma. This research was supported in part by a Grant-in-Aid for Scientific Research from Ministry of Education, Culture, Science, Sports, and Technology of Japan.

References

[1] H. Shi, Electrochim. Acta, 41 (1996)1639-1639.

[2] M. Endo, Y. J. Kim, H. Ohta, K. Ishii, T. Inoue, T. Hayashi, Y. Nishimura, T. Maeda, M. S. Dresselhaus, Carbon, 40 (2002) 2613-2626.

[3] J. Chmiola, G. Yushin. R. Dash, Y. Gogotsi, J. Power Sources, 158 (2006) 765-772.

[4] J. Gamby, P. L. Taberna, P. Simon, J. F. Fauvarque, M. Chesneau, J. Power Sources, 101 (2001) 109-116,.

[5] B. E. Conway, Electrochemical Supercapacitors, Plenum press, New York, 1999,

pp.186-193.

[6] B. E. Conway, Electrochemical Supercapacitors, Plenum press, New York, 1999, pp.199-203.

[7] C.-H. Kim, S.-I. Pyun, J.-H. Kim, Electrochim. Acta, 48 (2003) 3455-3463.

[8] I. Moriguchi, F. Nakahara, H. Yamada, T. Kudo, Electrochem. Solid-State Lett., 7 (2004) A221-A223.

[9] H. Yamada, H. Nakamura, F. Nakahara, I. Moriguchi, T. Kudo, J. Phys. Chem. C, 111 (2007) 227-233.

[10] H. Tamai, M. Kouzu, M. Morita, H. Yasuda, Electrochem. Solid-State Lett., 6 (2003) A214-A217.

[11] S Shiraishi, H. Kurihara, H. Tsubota, A. Oya, Y. Soneda, Y. Yamada, Electrochem. Solid-State Lett., 4 (2001) A5-A8.

[12] M. Ue, K. Ida, S. Mori, J. Electrochem. Soc., 141 (1994) 2989-2996.

[13] D. Lozano-Castelló, D. Cazorla-Amorós, A. Linares-Solano, S. Shiraishi, H. Kurihara, A. Oya, Carbon, 41 (2003) 1765-1775.

[14] J. Chmiola, G. Yushin, Y. Gogotsi, C. Portet, P. Simon, P. L. Taberna, Science, 313 (2006) 1760-1763.

[15] Deyang Qu, Hang Shi, J. Power Sources, 74 (1998) 99-107.

[16] L. Eliad, G. Salitra, A. Soffer, D. Aurbach, J. Phys. Chem. B, 105 (2001) 6880-6887.

[17] M. Ue, J. Electrochem. Soc. 141 (1994) 3336-3342.

[18] S. Kobayashi, Y. Uchimoto, J. Phys. Chem. B, 109 (2005) 13322.

[19] T. Abe, F. Sagane, M. Ohtsuka, Y. Iriyama, Z. Ogumi, J. Electrochem. Soc., 152 (2005) A2151.

[20] T. Ohkubo, T. Konishi, Y. Hattori, H. Kanoh, T. Fujikawa, K. Katsumi, J. Am. Chem. Soc. 124 (2002) 11860.

[21] K. Kaneko, Carbon, 38 (2000) 287.

Figure captions

Figure 1. N_2 adsorption/desorption isotherms at 77 K of the porous carbons. Solid and open symbols are of adsorption and desorption branches, respectively.

Figure 2. Pore size distribution of (a) mesopores and (b) micropores obtained by the BJH and HK method, respectively.

Figure 3. TEM images of the porous carbons: (a) C[110]-1, (b) C[17]-1 and (c) C[8]-1. (d) A high resolution image of C[17]-1.

Figure 4. Schematic hierarchical porous structure of the porous carbons synthesized by the colloidal-crystal-templating method.

Figure 5. Cyclic voltammograms of the hierarchical porous carbons.

Figure 6. Charge/discharge curves of the hierarchical porous carbons obtained by CC-CV mode at current densities of 0.05 to 10 A g^{-1}.

Figure 7. Plots of C_{DL}/S_{micro} vs. S_{meso}/S_{micro}.

Table 1. Specific surface areas and specific electric double layer capacitance (C_{DL}) of the porous carbons. (*a*) Total surface area, S_{total}, and meso-/macropore surface area, S_{meso}, were obtained from an α_{SPE}-plot and t-plot, respectively. Micropore surface area, S_{micro}, was calculated by subtracting S_{meso} from S_{total}. (*b*) R_s, electric series resistance, was estimated by extrapolation of the charge curves at 5 A g^{-1}. (*c*) C_{DL}, electric double layer capacitance, was obtained from the slope of the charge curves at 0.05 A g^{-1} and 5 A g^{-1}.

	Specific surface area (m^2 g^{-1}) [a]			R_s (Ω g) [b]	C_{DL} (F g^{-1}) [c]	
	S_{total}	S_{meso}	S_{micro}	@5 A g^{-1}	@0.05 A g^{-1}	@5 A g^{-1}
C[110]-1	1230	456	774	0.031	107	105
C[45]-1	1409	1060	349	0.050	116	117
C[45]-2	1204	711	493	-	96	-
C[17]-1	1302	801	501	0.053	104	94
C[17]-2	1455	986	469	-	119	-
C[8]-1	1153	806	347	0.079	95	93
C[8]-2	1089	791	298	-	94	-

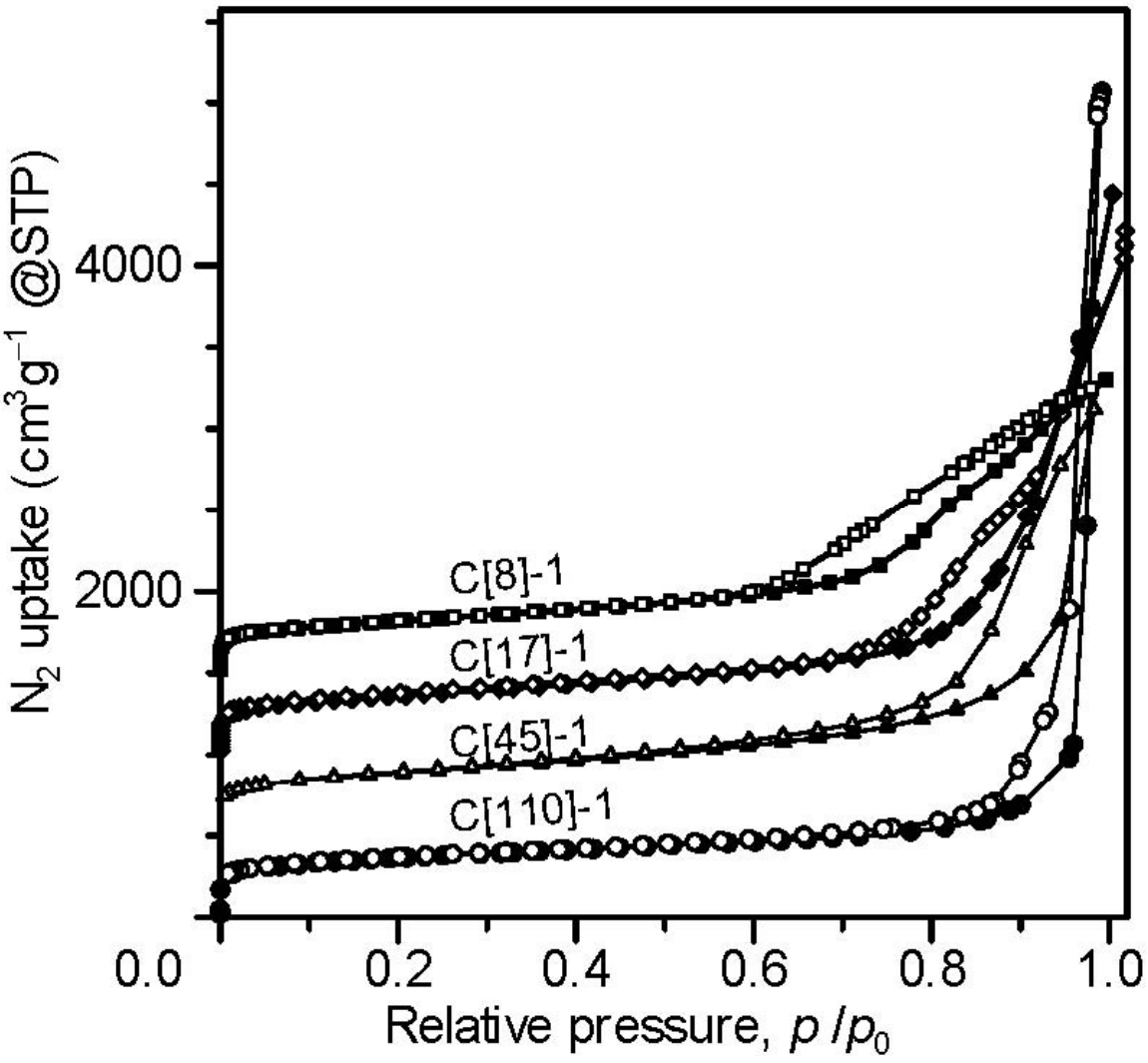
N_2 uptake (cm^3g^{-1} @STP)
4000
2000
C[8]-1
C[17]-1
C[45]-1
C[110]-1
0.0
0.2
0.4
0.6
0.8
1.0
Relative pressure, p/p_0

Fig. 1

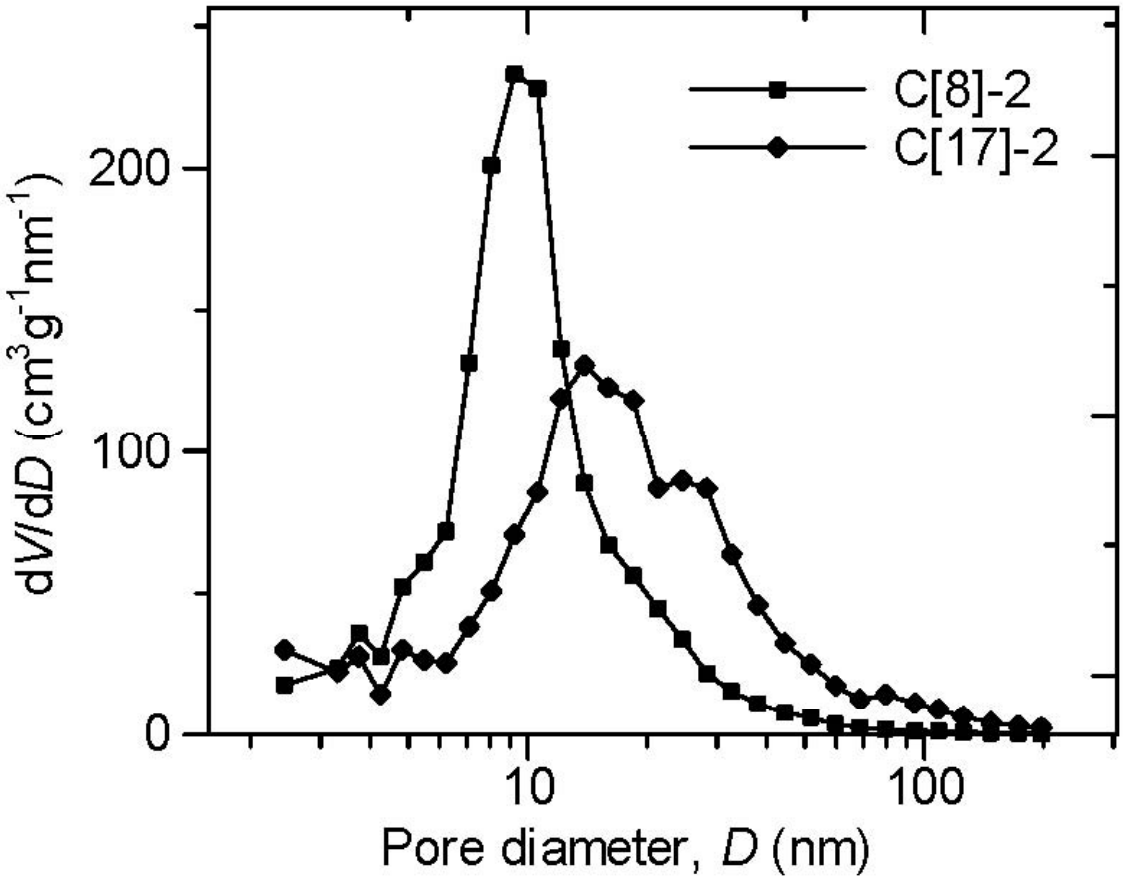

Fig. 2a

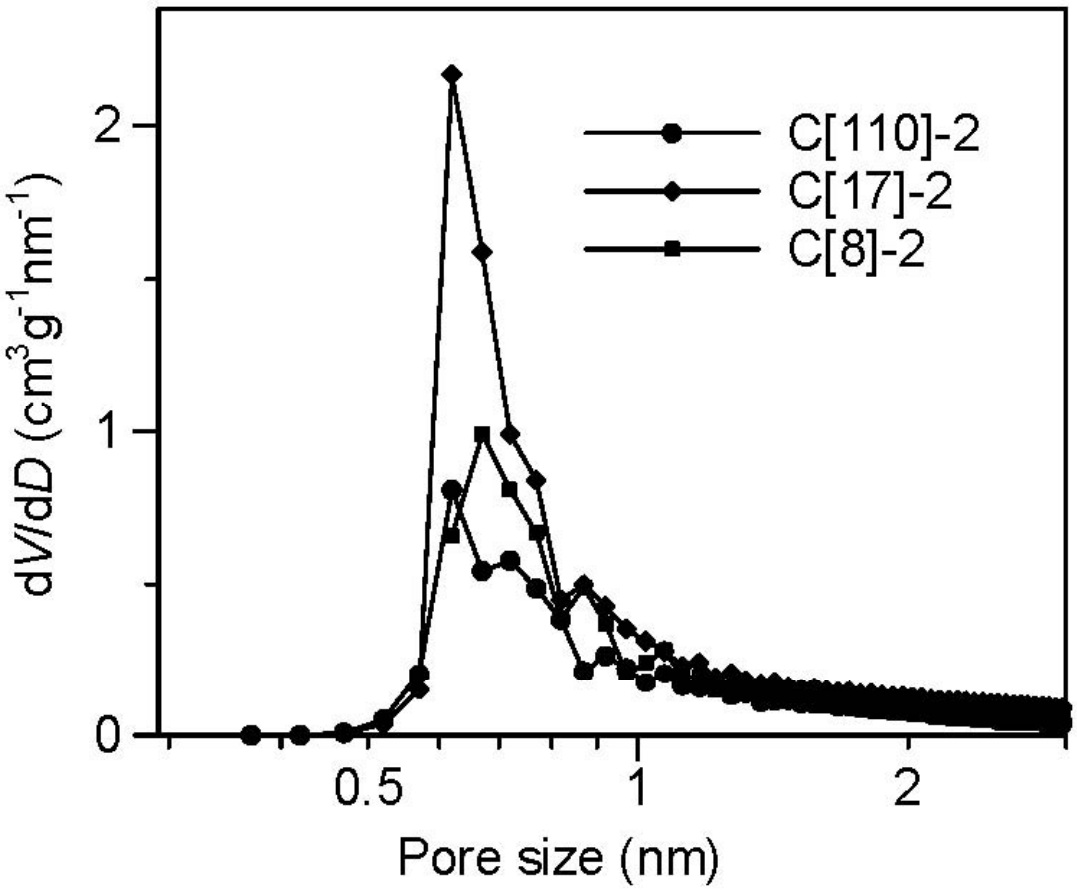

Fig. 2b

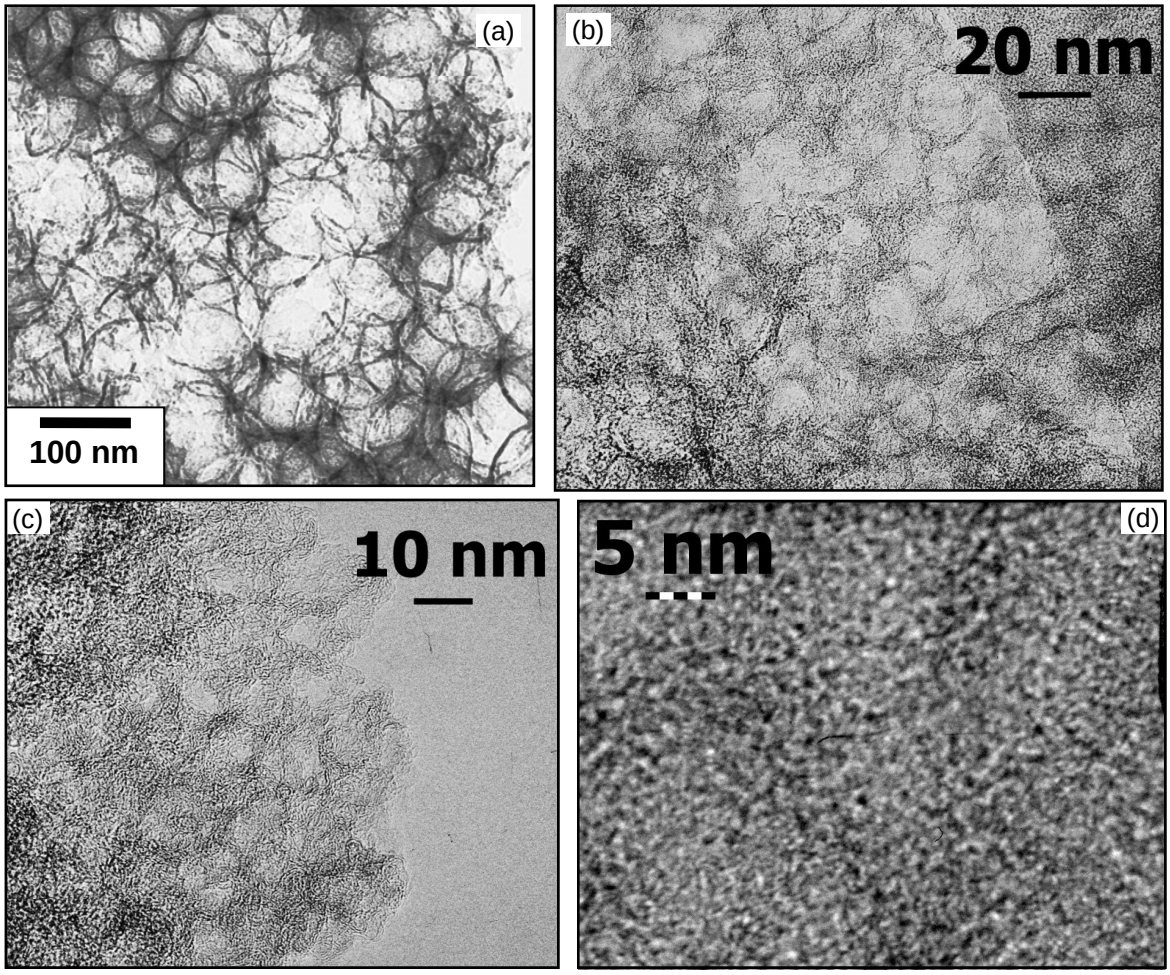

Fig. 3

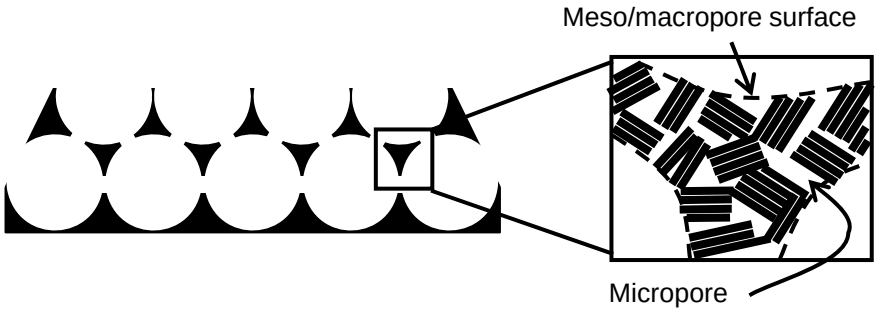

Fig. 4

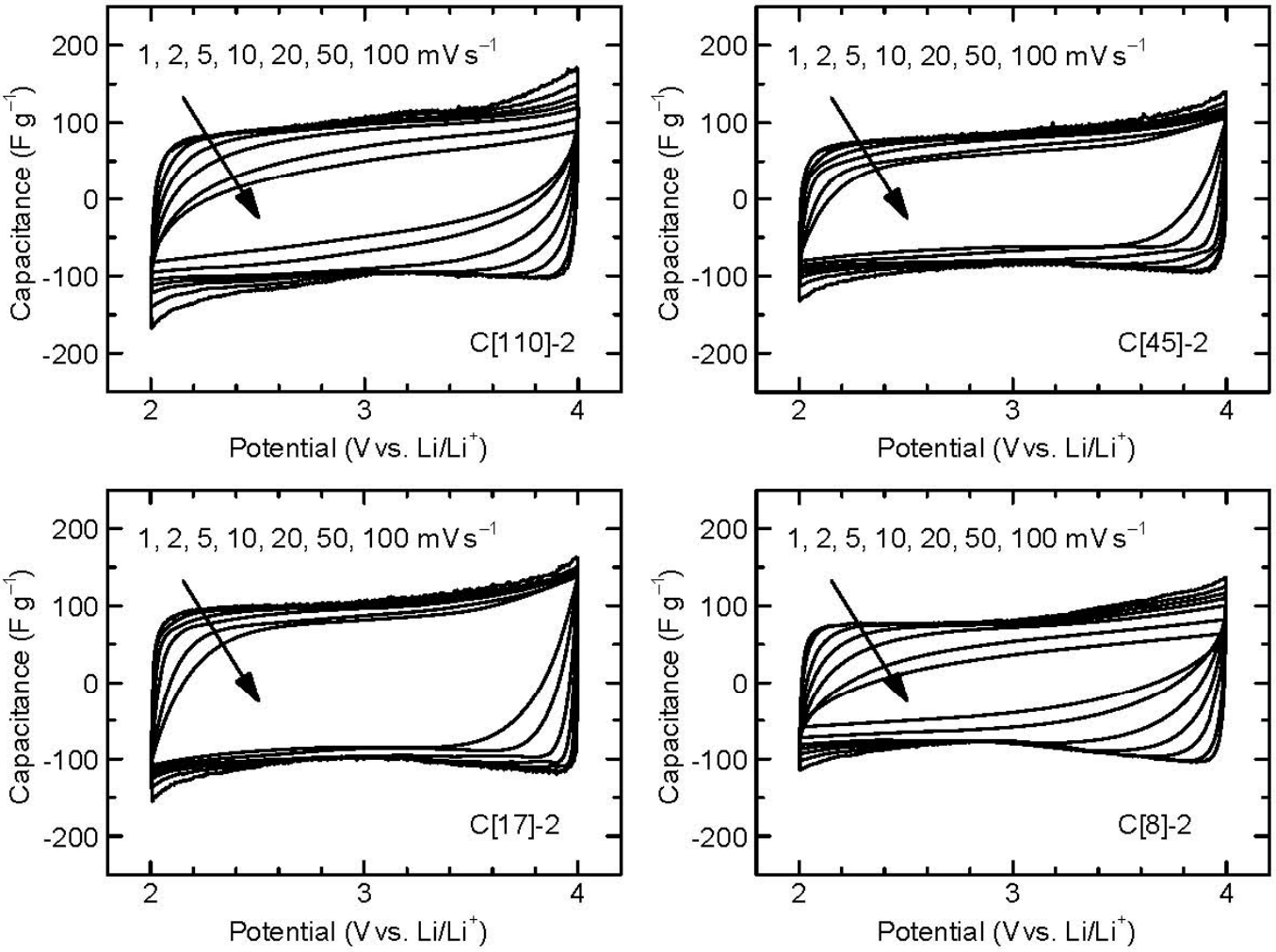
1, 2, 5, 10, 20, 50, 100 mV s^{-1}
C[110]-2
C[45]-2
C[17]-2
C[8]-2
Capacitance (F g^{-1})
Potential (V vs. Li/Li$^+$)
200
100
0
-100
-200
2
3
4

Fig. 5

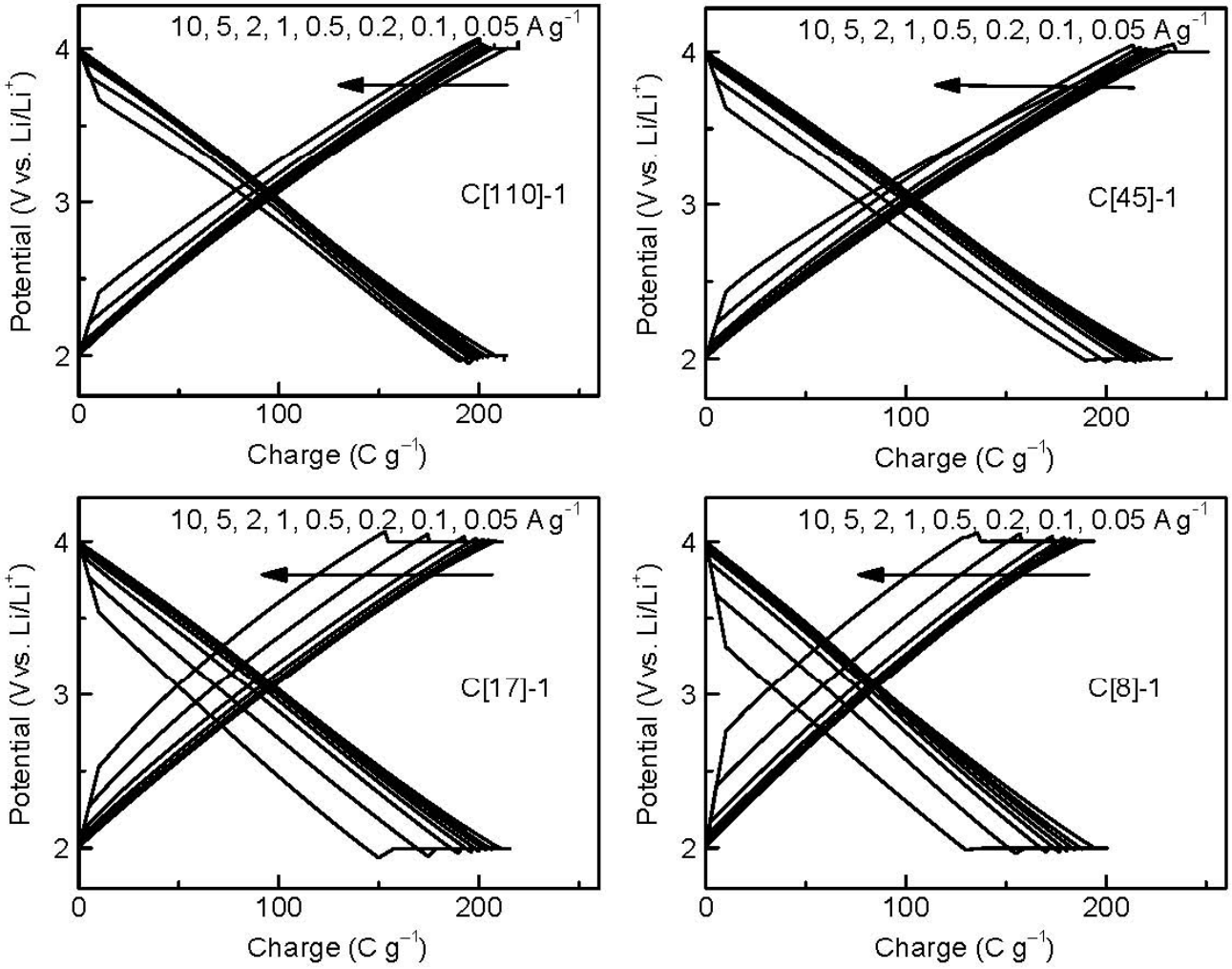
10, 5, 2, 1, 0.5, 0.2, 0.1, 0.05 A g-1
C[110]-1
C[45]-1
C[17]-1
C[8]-1
Potential (V vs. Li/Li+)
Charge (C g-1)
0
100
200
2
3
4

Fig. 6

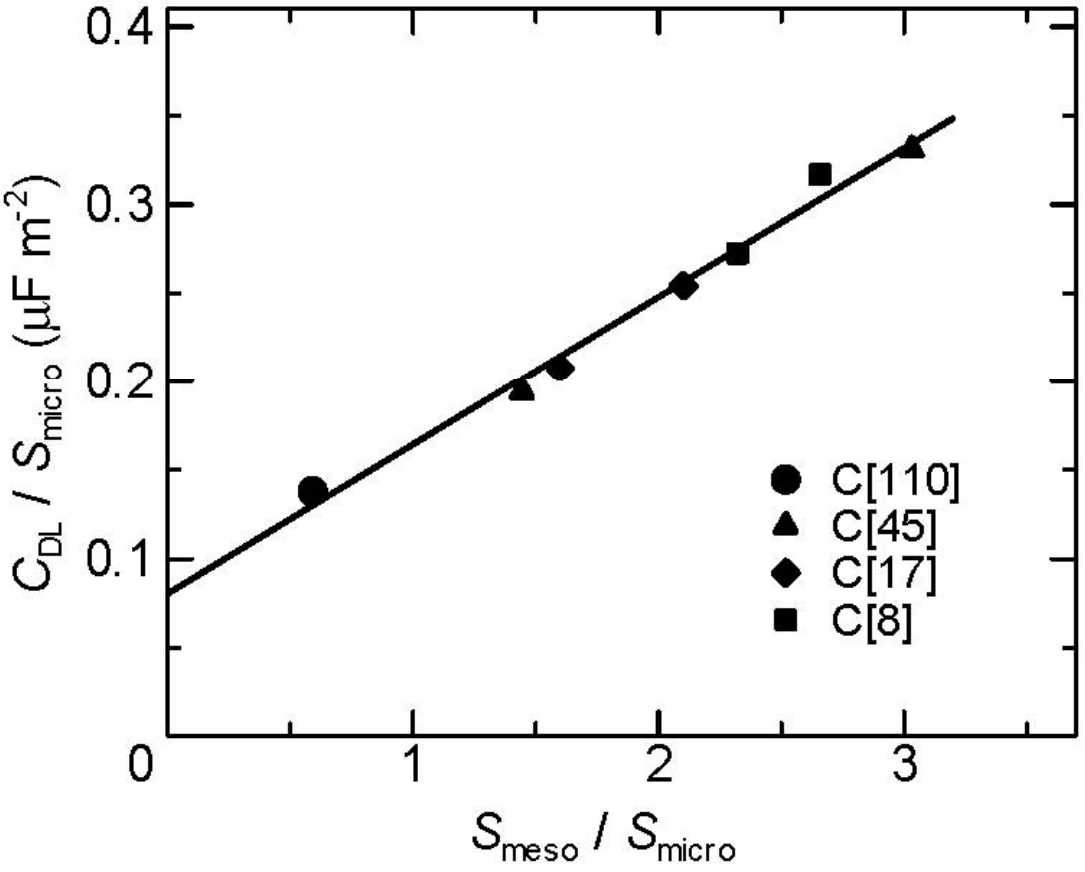

Fig. 7